Journal of
Applied and Computational Mechanics

Shahid Chamran
University of Ahvaz

Journal of Applied and Computational Mechanics

Research Paper

Bending of Functionally Graded Sandwich Nanoplates Resting on Pasternak Foundation under Different Boundary Conditions

Ahmed A. Daikh[1,2] , Ashraf M. Zenkour[3,4]

[1] Laboratoire d'Etude des Structures et de Mécanique des Matériaux, Department of Civil Engineering, Mascara, Algeria, Email: daikh.ahmed.amine@gmail.com

[2] Mechanics of Structures and Solids Laboratory, Faculty of Technology, University of Sidi Bel Abbes, Algeria

[3] Department of Mathematics, Faculty of Science, King Abdulaziz University, P.O. Box 80203, Jeddah 21589, Saudi Arabia, Email: zenkour@kau.edu.sa

[4] Department of Mathematics, Faculty of Science, Kafrelsheikh University, Kafrelsheikh 33516, Egypt, Email: zenkour@sci.kfs.edu.eg

Abstract. This article proposes a refined higher order nonlocal strain gradient theory for stresses and deflections of new model of functionally graded (FG) sandwich nanoplates resting on Pasternak elastic foundation. Material properties of the FG layers are supposed to vary continuously through-the-thickness according to a power function or a sigmoid function in terms of the volume fractions of the constituents. The face layers are made of FG material while the core layer is homogeneous and made of ceramic. In this study, an analytical approach is proposed using the higher-order shear deformation plate theory and nonlocal strain gradient theory with combination of various boundary conditions. Numerical outcomes are reported to display the impact of the material distribution, boundary conditions, elastic foundation parameters and the sandwich nanoplate geometry on the deflections and stresses of FG sandwich nanoplates. The exactness of this theory is determined by comparing it to other published outcomes.

Keywords: P-FGM, S-FGM, Sandwich nanoplates, Elastic foundation, Various boundary conditions.

1. Introduction

The functionally graded material (FGM) is a new class of advanced composite materials. The FGM is made of two mixed materials to obtain a synergistic combination of its mechanical and thermal properties [1]. These new materials are anticipated to decrease the local stress concentrations encouraged by abrupt transitions in material properties across the interface between separate materials [2]. Classically, FGMs are made of a ceramic and a metal for the resolution of thermal protection against large temperature gradients. Due to its low thermal conductivity, the ceramic has excellent characteristics in heat resistance. On the other hand, the ductile metal constituent avoids fracture due to its greater toughness. The synthesis of FGMs has been successfully demonstrated through a variety of methods, including thermal spray, powder metallurgy, physical and chemical vapor deposition and self-propagating high-temperature synthesis or combustion synthesis. High-temperature synthesis is particularly well suited to fabricating FGMs, because of the rapidity of the combustion reaction.

Sandwich structures have been widely used to solve several engineering problems such in areas of aircraft, automobile, aerospace, and shipbuilding due to their high strength and durability. To increase the material properties of sandwich structures, the FGMs are taken into account. In general, the unexpected variation in the material properties of the sandwich structures from one layer to another can result in stress concentrations that often result in delamination. To overcome this issue, the three-layer FG sandwich structure is anticipated due to the gradual distinction of material properties at the interfaces between its core and face layers.

Due to the importance and broad technical applications of smart composite pates, several researches are conducted on the mechanical response of FG sandwich plates. The stress distribution and deflection of simply supported FG sandwich plates are analyzed by Zenkour [3] using the third-order shear deformation plate theory (TSDT), the sinusoidal shear deformation plate theory (SSDT), the first-order shear deformation plate theory (FSDT) and the classical plate theory (CPT). In addition, by using a refined SSDT, he analyzed the effect of transverse mechanical and thermal load on the bending behavior of FG sandwich plates [4]. Wang and Shen [5] analyzed a nonlinear bending of FG sandwich plate resting on elastic foundations using a two-step perturbation method. Zenkour and Alghamdi [6-8] considered the thermoelastic bending of FG sandwich plates based on the higher-order shear deformation theories (HSDT). Two refined plate theories with four unknown variables are developed by Merdaci et al. [9] for static of FG sandwich plates. Natarajan and Ganapathi [10] examined the vibration and bending behavior of FG sandwich plates by employing QUAD-8 shear flexible element and in the context of HSDT. Iurlaro et al. [11] carried out bending and free vibration FG sandwich plates using a refined zigzag theory and finite element method. Thai et al. [12] examined bending, buckling and vibration of FG sandwich plates with various boundary conditions using a new FSDT. Mahi et al. [13] proposed a new hyperbolic shear deformation theory for the bending of FG sandwich plates. Using a new FSDT, Mantari and Granados [14] analyzed static bending

of sandwich plates with FG core and homogeneous face layers. Nguyen et al. [15] discussed the static and vibration of isotropic and FG sandwich plates by means of smooth finite element method and the HSDT with various boundary conditions. Mantari and Monge [16] carried out bending, buckling, and vibration of FG sandwich plates by employing an optimized hyperbolic unified formulation. Xiang and Liu [17] applied the nth-order shear deformation theory and meshless global collocation method for the bending analysis of FG sandwich plates with simply supported boundary conditions. Kashtalyan and co-workers [18, 19] investigated bending behavior of FG sandwich plates with FG core based on a three-dimensional elasticity solution. Abdelaziz et al. [20] analyzed the bending behavior of two types of FG sandwich plates based on four-variable refined plate theory. Using different four-variable refined plate theories, Li et al. [21] carried out bending of sandwich plates with both FG face layers and FG hard core subjected to thermomechanical loading.

Thanh et al. [22] examined static and dynamic behavior of laminated composite micro-plates using isogeometric analysis and a refined modified couple stress theory and considering account the small-scale effect. Phung-Van et al. [23] presented a generalized shear deformation theory in combination with isogeometric (IGA) approach for nonlinear transient analysis of smart piezoelectric FG plates subjected to thermoelectro-mechanical loads. Effect of porosities on static and free vibration response for FG nanoplates is studied by Phung-Van et al. [24] using the Eringen's nonlocal elasticity. The same authors [25] analyzed nonlinear transient responses of porous FG nanoplates using isogeometric analysis. Thai et al. [26] presented a size-dependent computational approach to analyze static bending and free vibration analyses of functionally graded carbon nanotube-reinforced composite (FG-CNTRC) plate based on the modified strain gradient theory and the HSDT. Thanh et al. [27] proposed a size-dependent model based on the modified couple stress theory and isogeometric analysis for static and free vibration behaviors of FG-CNTRC nanoplates using the higher order shear deformation theory. Neves et al. [28] investigated the bending behavior of a sandwich plate with FG core using a meshless technique and quasi-3D HSDT. Demirhan and Taskin [29] carried out bending of FG sandwich plates by employing Levy-type solution with state-space concept and four-variable refined plate theory. Applying the mesh-free method and FSDT, Moradi-Dastjerdi and Aghadavoudi [30] studied the bending response of sandwich plates with FG nanocomposite face layers reinforced by three types of defected carbon nanotubes and resting on elastic foundation. Li et al. [31] examined a novel type of FG plates under transverse distributed loadings. Thai et al. [32] used a four-unknown shear deformable model for static bending, free vibration and buckling behavior of isotropic and sandwich FG microplates based on the modified strain gradient theory. Phung-Van et al. [33] investigated nonlinear transient dynamic of FG-CNTRC nanoplates subjected to a transverse uniform load in thermal environments. Size-dependent impact on thermal buckling and post-buckling response of imperfect FG micro-plates is examined by Thanh et al. [34] using seventh-order shear deformation plate theory associated with the modified couple stress theory. The porosity impact on bending response of two types of FG sandwich plates is analyzed by Daikh and Zenkour [35] using a new higher shear deformation theory.

Numerous researches are performed for FGM plates with complex geometries. For example, Cao et al. [36] proposed a semi-analytical graded FEM to analyze FGM plates with complex shapes and holes. The effect of elliptic Hole geometry and thermal Loads on buckling of FG plates subjected to various boundary conditions is carried out by Rezaei et al. [37]. Yang et al. [38] employed 3D elasticity solutions to study equilibrium problems of transversely isotropic FGM plates with holes. They have also used the same solutions for isotropic FGM plates with an elliptical hole [39]. Several researchers studied deflection of FGM nanoplates [40-45], but there are no research papers examined the effect of size dependent on the axial and shear stresses.

The main purpose of this article is to examine the deflection and stresses of FG nanoplates using a refined fifth-order shear deformation theory with combination of the nonlocal strain gradient theory. A new model of FG sandwich plates based on sigmoid function is presented and analyzed. The equilibrium and stability equations for FG plates are gained in the context of the refined HSDT. Governing equations are analyzed for the presented sandwich plate under various boundary conditions. The effect of nonlocal parameters on the axial and shear stresses of FG sandwich plates is analyzed here for the first time.

2. FG Sandwich Plates

In this research, we proposed the sandwich nanoplate as composed of two FG face layers (metal-ceramic) and isotropic homogeneous core (ceramic) as shown in Fig. 1. The vertical positions of the bottom face of the sandwich, the two interfaces, and the top face are $h_0 = -h/2$, h_1, h_2 and $h_3 = h/2$, respectively. Two models of sandwich nanoplates are used: power-law functionally graded sandwich plates P-FGSP and sigmoid functionally graded sandwich plates S-FGSP.

2.1 Power-law functionally graded sandwich plate (P-FGSP)

The sandwich plate is composed of two power-law FG face layers that are graded from metal to ceramic while the core layer is made of ceramic. The volume fraction $V^{(n)}$ of layer n $(n = 1,2,3)$, varies through-the-thickness of the sandwich according to power-law function as follows

$$
\begin{aligned}
V^{(1)}(z) &= \left(\frac{z-h_0}{h_1-h_0}\right)^p, \quad h_0 \le z \le h_1, \\
V^{(2)}(z) &= 1, \quad h_1 \le z \le h_2, \\
V^{(3)}(z) &= \left(\frac{z-h_3}{h_2-h_3}\right)^p, \quad h_2 \le z \le h_3,
\end{aligned}
\tag{1}
$$

where parameter $p \ge 0$ denotes volume fraction index.
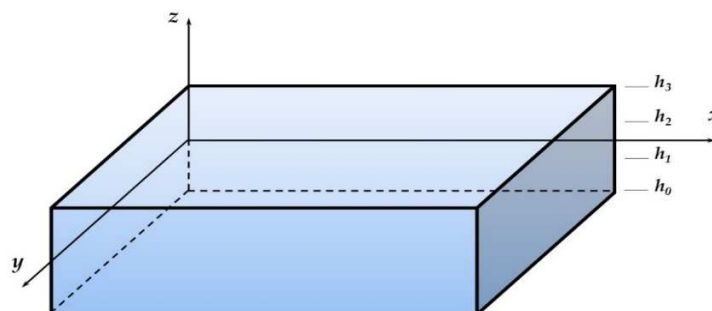

Fig. 1. Coordinate system and geometry of the FG sandwich plate

2.2 Sigmoid functionally graded sandwich plate (S-FGSP)

The volume fraction of this sandwich model varies according to a sigmoid function through-the-thickness as follows

$$
\begin{aligned}
V_1^{(1)}(z) &= \tfrac{1}{2}\left(\frac{z-h_0}{h_m-h_0}\right)^p, \quad h_0 \leq z \leq h_m, \\
V_2^{(1)}(z) &= 1 - \tfrac{1}{2}\left(\frac{z-h_1}{h_m-h_1}\right)^p, \quad h_m \leq z \leq h_1, \\
V^{(2)}(z) &= 1, \quad h_1 \leq z \leq h_2, \\
V_1^{(3)}(z) &= 1 - \tfrac{1}{2}\left(\frac{z-h_2}{h_n-h_2}\right)^p, \quad h_2 \leq z \leq h_n, \\
V_2^{(3)}(z) &= \tfrac{1}{2}\left(\frac{z-h_3}{h_n-h_3}\right)^p, \quad h_n \leq z \leq h_3,
\end{aligned}
\tag{2}
$$

where $h_m = (h_1 + h_2)/2$ and $h_n = (h_2 + h_3)/2$ represents the mid-surface positions of the bottom and the top layers, respectively.

3. Kinematics and constitutive equations

3.1 Nonlocal strain gradient elasticity theory

By the coupling physical influences of the strain gradient stress and nonlocal elastic stress fields, the stress proposed by Lim et al. [46] can be written as:

$$
\sigma_{ij} = \sigma_{ij}^{(0)} - \frac{d\sigma_{ij}^{(1)}}{dx}
\tag{3}
$$

where $\sigma_{ij}^{(0)}$ and $\sigma_{ij}^{(1)}$ are the classical stress corresponds to strain ε_{kl} and the higher-order stress $\sigma_{ij}^{(1)}$ corresponds to strain gradient $\varepsilon_{kl,x}$ respectively, and can be expressed as

$$
\sigma_{ij}^{(0)} = \int_0^L C_{ijkl}\alpha_0(x,x',e_0a)\varepsilon_{kl,x}(x')dx'
\tag{4}
$$

$$
\sigma_{ij}^{(1)} = l^2 \int_0^L C_{ijkl}\alpha_1(x,x',e_1a)\varepsilon_{kl,x}(x')dx'
\tag{5}
$$

where C_{ijkl} are elastic constants and l is the material length scale parameter presented to reflect the significance of the strain gradient stress field. e_0a and e_1a are the nonlocal parameters presented to reflect the significance of the nonlocal elastic stress field.

The nonlocal kernel functions $\alpha_0(x,x',e_0a)$ and $\alpha_1(x,x',e_1a)$ gratify the developed conditions by Eringen [47]. The general constitutive relation become as

$$
[1-(e_1a)^2\nabla^2][1-(e_0a)^2\nabla^2]\sigma_{ij} = C_{ijkl}[1-(e_1a)^2\nabla^2]\varepsilon_{kl} - C_{ijkl}l^2[1-(e_0a)^2\nabla^2]\nabla^2\varepsilon_{kl}
\tag{6}
$$

where ∇^2 denotes the Laplacian operator. In the current analysis, we assume the coefficient $e = e_0 = e_1$. The total nonlocal strain gradient constitutive relations can be stated as [48]

$$
[1-\mu\nabla^2]\sigma_{ij} = C_{ijkl}[1-\lambda\nabla^2]\varepsilon_{kl}
\tag{7}
$$

where $\mu = (ea)^2$ and $\lambda = l^2$.

3.2 Higher-order plate theory

Let us consider a rectangular sandwich nanoplate of length a, width b, and thickness h. The displacement components of the HSDT are

$$
\begin{aligned}
u(x,y,z) &= u_0 - z\frac{\partial w_0}{\partial x} + \Psi(z)\varphi_1, \\
v(x,y,z) &= v_0 - z\frac{\partial w_0}{\partial y} + \Psi(z)\varphi_2, \\
w(x,y,z) &= w_0,
\end{aligned}
\tag{9}
$$

where (u_0, v_0, w_0) and (φ_1, φ_2) refer to the displacement and rotation of transverse normal on the plane $z = 0$, respectively. $\Psi(z)$ represents the function in a way that regulates the distribution of the transverse shear strains and stresses across the thickness of the nanoplate. For example, Reddy [49] attained the displacements by putting $\Psi(z) = z\left(1 - \frac{4z^2}{3h^2}\right)$, and Touratier [50] anticipated the SSDT by putting $\Psi(z) = \frac{h}{\pi}\sin\left(\frac{z}{h}\right)$. The displacements for the CPT is gained by setting $\Psi(z) = 0$, and $\Psi(z) = z$ for the FSDT.

3.3 Refined plate theory

Based on the assumptions given by Senthilnathan et al. [51], the displacement fields of four variable shear deformation plate theories are given as

$$
\begin{aligned}
u(x,y,z) &= u_0 - z\frac{\partial w_b}{\partial x} - f(z)\frac{\partial w_s}{\partial x}, \\
v(x,y,z) &= v_0 - z\frac{\partial w_b}{\partial y} - f(z)\frac{\partial w_s}{\partial y}, \\
w(x,y,z) &= w_b + w_s.
\end{aligned}
\tag{10}
$$

where w_b denotes the bending component of the transverse displacement w and w_s is the shear component. The displacement of the new refined plate theory is obtained by setting

$$
f(z) = \frac{3z^3}{2h^2} - \frac{2z^5}{5h^4}.
\tag{11}
$$

The strains associated with the displacements can be given as

$$\begin{Bmatrix} \varepsilon_{xx} \\ \varepsilon_{yy} \\ \gamma_{xy} \end{Bmatrix} = \begin{Bmatrix} \varepsilon_{xx}^0 \\ \varepsilon_{yy}^0 \\ \gamma_{xy}^0 \end{Bmatrix} + z \begin{Bmatrix} \varepsilon_{xx}^1 \\ \varepsilon_{yy}^1 \\ \gamma_{xy}^1 \end{Bmatrix} + f(z) \begin{Bmatrix} \varepsilon_{xx}^2 \\ \varepsilon_{yy}^2 \\ \gamma_{xy}^2 \end{Bmatrix},$$

$$\varepsilon_{zz} = 0, \quad \begin{Bmatrix} \gamma_{yz} \\ \gamma_{xz} \end{Bmatrix} = \left[1 - \frac{df(z)}{dz} \right] \begin{Bmatrix} \gamma_{yz}^0 \\ \gamma_{xz}^0 \end{Bmatrix},$$

(12)

where

$$\begin{Bmatrix} \varepsilon_{xx}^0 \\ \varepsilon_{yy}^0 \\ \gamma_{xy}^0 \end{Bmatrix} = \begin{Bmatrix} \frac{\partial u_0}{\partial x} \\ \frac{\partial v_0}{\partial y} \\ \frac{\partial v_0}{\partial x} + \frac{\partial u_0}{\partial y} \end{Bmatrix}, \quad \begin{Bmatrix} \varepsilon_{xx}^1 \\ \varepsilon_{yy}^1 \\ \gamma_{xy}^1 \end{Bmatrix} = - \begin{Bmatrix} \frac{\partial^2 w_b}{\partial x^2} \\ \frac{\partial^2 w_b}{\partial y^2} \\ 2\frac{\partial^2 w_b}{\partial x \partial y} \end{Bmatrix},$$

$$\begin{Bmatrix} \varepsilon_{xx}^2 \\ \varepsilon_{yy}^2 \\ \gamma_{xy}^2 \end{Bmatrix} = - \begin{Bmatrix} \frac{\partial^2 w_s}{\partial x^2} \\ \frac{\partial^2 w_s}{\partial y^2} \\ 2\frac{\partial^2 w_s}{\partial x \partial y} \end{Bmatrix}, \quad \begin{Bmatrix} \gamma_{yz}^0 \\ \gamma_{xz}^0 \end{Bmatrix} = \begin{Bmatrix} \frac{\partial w_s}{\partial x} \\ \frac{\partial w_s}{\partial y} \end{Bmatrix}.$$

(13)

Now, the constitutive equations of the FG sandwich nanoplate can be expressed as

$$[1 - \mu \nabla^2] \begin{Bmatrix} \sigma_{xx} \\ \sigma_{yy} \\ \sigma_{yz} \\ \sigma_{xz} \\ \sigma_{xy} \end{Bmatrix}^{(n)} = [1 - \lambda \nabla^2] \begin{bmatrix} Q_{11} & Q_{12} & 0 & 0 & 0 \\ Q_{12} & Q_{22} & 0 & 0 & 0 \\ 0 & 0 & Q_{44} & 0 & 0 \\ 0 & 0 & 0 & Q_{55} & 0 \\ 0 & 0 & 0 & 0 & Q_{66} \end{bmatrix}^{(n)} \begin{Bmatrix} \varepsilon_{xx} \\ \varepsilon_{yy} \\ \gamma_{yz} \\ \gamma_{xz} \\ \gamma_{xy} \end{Bmatrix},$$

(14)

where

$$Q_{11}^{(n)} = Q_{22}^{(n)} = \frac{E^{(n)}(z)}{1-\nu^{(n)2}}, \quad Q_{12}^{(n)} = \nu Q_{11}^{(n)}, \quad Q_{44}^{(n)} = Q_{55}^{(n)} = Q_{66}^{(n)} = \frac{E^{(n)}(z)}{2(1+\nu^{(n)})}.$$

(15)

4. Governing Equations

By applying the principle of virtual work, equilibrium equations associated with the present problem will be obtained as

$$\frac{\partial N_{xx}}{\partial x} + \frac{\partial N_{xy}}{\partial y} = 0,$$

$$\frac{\partial N_{xy}}{\partial x} + \frac{\partial N_{yy}}{\partial y} = 0,$$

$$\frac{\partial^2 M_{xx}^b}{\partial x^2} + 2\frac{\partial^2 M_{xy}^b}{\partial x \partial y} + \frac{\partial^2 M_{yy}^b}{\partial y^2} + q - R = 0,$$

$$\frac{\partial^2 M_{xx}^s}{\partial x^2} + 2\frac{\partial^2 M_{xy}^s}{\partial x \partial y} + \frac{\partial^2 M_{yy}^s}{\partial y^2} + \frac{\partial R_{xz}^s}{\partial x} + \frac{\partial R_{yz}^s}{\partial y} + q - \Re = 0.$$

(16)

The density of reaction of the foundation $\Re$ and the transverse displacement w relationship is given by

$$\Re = K_w w - K_g \nabla^2 w$$

(17)

K_w and K_g are the Winkler's (normal) and Pasternak's (shear) foundation stiffnesses and ∇^2 is the Laplace operator in x and y. Also, the stress resultants N, M and R are defined as

$$\begin{Bmatrix} N_{xx} \\ N_{yy} \\ N_{xy} \end{Bmatrix} = \sum_{n=1}^3 \int_{h_{n-1}}^{h_n} \begin{Bmatrix} \sigma_{xx} \\ \sigma_{yy} \\ \sigma_{xy} \end{Bmatrix}^{(n)} dz, \quad \begin{Bmatrix} M_{xx}^b \\ M_{yy}^b \\ M_{xy}^b \end{Bmatrix} = \sum_{n=1}^3 \int_{h_{n-1}}^{h_n} \begin{Bmatrix} \sigma_{xx} \\ \sigma_{yy} \\ \sigma_{xy} \end{Bmatrix}^{(n)} z\, dz,$$

$$\begin{Bmatrix} M_{xx}^s \\ M_{yy}^s \\ M_{xy}^s \end{Bmatrix} = \sum_{n=1}^3 \int_{h_{n-1}}^{h_n} \begin{Bmatrix} \sigma_{xx} \\ \sigma_{yy} \\ \sigma_{xy} \end{Bmatrix}^{(n)} f(z)\, dz, \quad \begin{Bmatrix} R_{yz}^s \\ R_{xz}^s \end{Bmatrix} = \sum_{n=1}^3 \int_{h_{n-1}}^{h_n} \begin{Bmatrix} \sigma_{yz} \\ \sigma_{xz} \end{Bmatrix}^{(n)} \frac{df(z)}{dz}\, dz.$$

(18)

The stress resultants of the nanoplate can be connected to the total strains by

$$[1 - \mu \nabla^2] \begin{Bmatrix} \{N\} \\ \{M^b\} \\ \{M^s\} \end{Bmatrix} = [1 - \lambda \nabla^2] \begin{bmatrix} [A] & [B] & [B^s] \\ [B] & [D] & [D^s] \\ [B^s] & [D^s] & [H^s] \end{bmatrix} \begin{Bmatrix} \{\varepsilon^0\} \\ \{\varepsilon^1\} \\ \{\varepsilon^2\} \end{Bmatrix},$$

$$[1 - \mu \nabla^2] \begin{Bmatrix} R_{yz}^s \\ R_{xz}^s \end{Bmatrix} = [1 - \lambda \nabla^2] \begin{bmatrix} J_{44} & 0 \\ 0 & J_{55} \end{bmatrix} \begin{Bmatrix} \gamma_{yz}^0 \\ \gamma_{xz}^0 \end{Bmatrix},$$

(19)

where

$$\{N\} = \{N_{xx} \quad N_{yy} \quad N_{xy}\}^T, \quad \{M^b\} = \{M_{xx}^b, M_{yy}^b, M_{xy}^b\}^T,$$

$$\{M^s\} = \{M_{xx}^s, M_{yy}^s, M_{xy}^s\}^T,$$

(20)

$$\{\varepsilon^0\} = \{\varepsilon_{xx}^0 \quad \varepsilon_{yy}^0 \quad \gamma_{xy}^0\}^T, \quad \{\varepsilon^1\} = \{\varepsilon_{xx}^1 \quad \varepsilon_{yy}^1 \quad \gamma_{xy}^1\}^T,$$

$$\{\varepsilon^2\} = \{\varepsilon_{xx}^2 \quad \varepsilon_{yy}^2 \quad \gamma_{xy}^2\}^T,$$

(21)

$$A = \begin{bmatrix} A_{11} & A_{12} & 0 \\ A_{12} & A_{22} & 0 \\ 0 & 0 & A_{66} \end{bmatrix}, \quad B = \begin{bmatrix} B_{11} & B_{12} & 0 \\ B_{12} & B_{22} & 0 \\ 0 & 0 & B_{66} \end{bmatrix}, \quad D = \begin{bmatrix} D_{11} & D_{12} & 0 \\ D_{12} & D_{22} & 0 \\ 0 & 0 & D_{66} \end{bmatrix},$$

$$B^s = \begin{bmatrix} B_{11}^s & B_{12}^s & 0 \\ B_{12}^s & B_{22}^s & 0 \\ 0 & 0 & B_{66}^s \end{bmatrix}, \quad D^s = \begin{bmatrix} D_{11}^s & D_{12}^s & 0 \\ D_{12}^s & D_{22}^s & 0 \\ 0 & 0 & D_{66}^s \end{bmatrix}, \quad H^s = \begin{bmatrix} H_{11}^s & H_{12}^s & 0 \\ H_{12}^s & H_{22}^s & 0 \\ 0 & 0 & H_{66}^s \end{bmatrix}. \tag{22}$$

Here A_{ij}, B_{ij},..., H_{ij} are the nanoplate stiffness, defined by

$$\{A_{ij}, B_{ij}, D_{ij}, B_{ij}^s, D_{ij}^s, H_{ij}^s\} = \sum_{n=1}^{3} \int_{h_{n-1}}^{h_n} Q_{ij}^{(n)} \{1, z, z^2, f(z), zf(z), f(z)^2\} \mathrm{d}z,$$

$$J_{kk} = \sum_{n=1}^{3} \int_{h_{n-1}}^{h_n} Q_{kk}^{(n)} \left[\frac{\mathrm{d}f(z)}{\mathrm{d}z}\right]^2 \mathrm{d}z, \quad (i,j = 1,2,6, k = 4,5). \tag{23}$$

5. Exact Solutions for FG Sandwich Plates

The analytical solution of the governing equations for bending of sandwich nanoplate with simply-supported (S) or clamped (C) edges or combinations of them is presented. The boundary conditions are given as:

- Simply supported:

$$v_0 = w_b = w_s = \frac{\partial w_s}{\partial y} = \frac{\partial w_b}{\partial y} = 0 \quad \text{at} \quad x = 0, a,$$

$$u_0 = w_b = w_s = \frac{\partial w_s}{\partial x} = \frac{\partial w_b}{\partial x} = 0 \quad \text{at} \quad y = 0, b. \tag{24}$$

- Clamped:

$$u_0 = v_0 = w_b = w_s = \frac{\partial w_s}{\partial x} = \frac{\partial w_s}{\partial y} = \frac{\partial w_b}{\partial x} = \frac{\partial w_b}{\partial y} = 0 \quad \text{at} \quad x = 0, a \text{ and } y = 0, b. \tag{25}$$

The displacement field satisfying the above boundary conditions can be assumed as

$$u_0 = \sum_{m=1}^{\infty} \sum_{n=1}^{\infty} U_{mn} \frac{\partial X_m(x)}{\partial x} Y_n(y),$$

$$v_0 = \sum_{m=1}^{\infty} \sum_{n=1}^{\infty} V_{mn} X_m(x) \frac{\partial Y_n(y)}{\partial y},$$

$$w_b = \sum_{m=1}^{\infty} \sum_{n=1}^{\infty} W_{bmn} X_m(x) Y_n(y),$$

$$w_s = \sum_{m=1}^{\infty} \sum_{n=1}^{\infty} W_{smn} X_m(x) Y_n(y), \tag{26}$$

Here, U_{mn}, V_{mn}, W_{mn}^b and W_{mn}^s are arbitrary parameters. q_0 denotes the intensity of the load at the nanoplate center. m and n are mode numbers. The functions $X_m(x)$ and $Y_n(y)$ which satisfy the above boundary conditions are given as

- SSSS:

$$X_m(x) = \sin(\alpha x), \quad Y_n(y) = \sin(\beta y). \tag{27}$$

- CCCC:

$$X_m(x) = \sin^2(\alpha x), \quad Y_n(y) = \sin^2(\beta y). \tag{28}$$

- CCSS:

$$X_m(x) = \sin^2(\alpha x), \quad Y_n(y) = \sin(\beta y). \tag{29}$$

- CSCS:

$$X_m(x) = \sin(\alpha x)[\cos(\alpha x) - 1], \quad Y_n(y) = \sin(\beta y)[\cos(\beta y) - 1]. \tag{30}$$

where $\lambda = m\pi/a$, $\mu = n\pi/b$. By substituting eqs. (27-30) in eq. (16), one obtains

$$[L]\{\Lambda\} = \{F\}, \tag{31}$$

where $\{\Lambda\}$ and $\{F\}$ denotes the columns and [L] is a matrix

$$\{\Lambda\} = \{U, V, W_b, W_s\}^T, \tag{32}$$

$$\{F\} = \{0, 0, 0, f_q\}^T, \tag{33}$$

where the sinusoidal applied load can be written as [52]

$$f_q = -q_0 \int_0^a \int_0^b \sin^2(\alpha x) \sin^2(\beta y) \, \mathrm{d}x\mathrm{d}y - \mu q_0 \left[\int_0^a \int_0^b \alpha^2 \sin^3(\alpha x) \sin^2(\beta y) \, \mathrm{d}x\mathrm{d}y \right.$$

$$\left. + \int_0^a \int_0^b \beta^2 \sin^2(\alpha x) \sin^2(\beta y) \, \mathrm{d}x\mathrm{d}y\right]. \tag{34}$$

The elements L_{ij} of the matrix [L] are given by

$$L_{11} = A_{11}\alpha_{12} + A_{66}\alpha_8 - \lambda[A_{11}\alpha_{14} + (A_{66} + A_{11})\alpha_{15} + A_{66}\alpha_{16}],$$

$$L_{12} = \alpha_8(A_{12} + A_{66}) - \lambda[(\alpha_{15} + \alpha_{16})(A_{12} + A_{66})],$$

$$L_{13} = -B_{11}\alpha_{12} - \alpha_8(B_{12} + 2B_{66}) + \lambda[B_{11}\alpha_{14} + \alpha_{15}(B_{12} + 2B_{66} + B_{11}) + \alpha_{16}(B_{12} + 2B_{66})],$$

$$L_{14} = -B_{11}^s\alpha_{12} - \alpha_8(B_{12}^s + 2B_{66}^s) + \lambda[B_{11}^s\alpha_{14} + \alpha_{15}(B_{12}^s + 2B_{66}^s + B_{11}^s) + \alpha_{16}(B_{12}^s + 2B_{66}^s)],$$

$$L_{21} = \alpha_{10}(A_{12} + A_{66}) - \lambda[(\alpha_{17} + \alpha_{18})(A_{12} + A_{66})],$$

$$L_{22} = A_{66}\alpha_4 + A_{22}\alpha_{10} - \lambda[(A_{22} + A_{66})\alpha_{18} + A_{22}\alpha_{17} + A_{66}\alpha_{19}],$$

$$L_{23} = -B_{22}\alpha_4 - \alpha_{10}(B_{12} + 2B_{66}) + \lambda[\alpha_{17}(B_{12} + 2B_{66}) + \alpha_{18}(B_{12} + 2B_{66} + B_{22}) + B_{22}\alpha_{19}],$$

$$L_{24} = -B_{22}^s\alpha_4 - \alpha_{10}(B_{12}^s + 2B_{66}^s) + \lambda[\alpha_{17}(B_{12}^s + 2B_{66}^s) + \alpha_{18}(B_{12}^s + 2B_{66}^s + B_{22}^s) + B_{22}^s\alpha_{19}],$$

$$L_{31} = -B_{11}\alpha_{13} - \alpha_{11}(B_{12} + 2B_{66}) + \lambda[B_{11}\alpha_{22} + \alpha_{20}(B_{12} + 2B_{66} + B_{11}) + \alpha_{21}(B_{12} + 2B_{66})],$$

$$L_{32} = -B_{22}\alpha_5 - \alpha_{11}(B_{12} + 2B_{66}) + \lambda[\alpha_{20}(B_{12} + 2B_{66}) + \alpha_{21}(B_{12} + 2B_{66} + B_{22}) + B_{22}\alpha_{23}],$$

$$L_{33} = D_{11}\alpha_{13} + (2D_{12} + 4D_{66})\alpha_{11} + D_{22}\alpha_5$$
$$-\lambda[D_{11}\alpha_{22} + (2D_{12} + 4D_{66} + D_{11})\alpha_{20} + (2D_{12} + 4D_{66} + D_{22})\alpha_{21} + D_{22}\alpha_{23}]$$
$$-K_w\alpha_1 + K_g(\alpha_3 + \alpha_9) - \mu[-K_w\alpha_9 + K_g(\alpha_{11} + \alpha_{13}) - K_w\alpha_3 + K_g(\alpha_5 + \alpha_{11})],$$

$$L_{34} = D_{11}^s\alpha_{13} + (2D_{12}^s + 4D_{66}^s)\alpha_{11} + D_{22}^s\alpha_5$$
$$-\lambda[D_{11}^s\alpha_{22} + (2D_{12}^s + 4D_{66}^s + D_{11}^s)\alpha_{20} + (2D_{12}^s + 4D_{66}^s + D_{22}^s)\alpha_{21} + D_{22}^s\alpha_{23}]$$
$$-K_w\alpha_1 + K_g(\alpha_3 + \alpha_9) - \mu[-K_w\alpha_9 + K_g(\alpha_{11} + \alpha_{13}) - K_w\alpha_3 + K_g(\alpha_5 + \alpha_{11})],$$

$$L_{41} = -B_{11}^s\alpha_{13} - \alpha_{11}(B_{12}^s + 2B_{66}^s) + \lambda[B_{11}^s\alpha_{22} + \alpha_{20}(B_{12}^s + 2B_{66}^s + B_{11}^s) + \alpha_{21}(B_{12}^s + 2B_{66}^s)],$$

$$L_{42} = -B_{22}^s\alpha_5 - \alpha_{11}(B_{12}^s + 2B_{66}^s) + \lambda[\alpha_{20}(B_{12}^s + 2B_{66}^s) + \alpha_{21}(B_{12}^s + 2B_{66}^s + B_{22}^s) + B_{22}^s\alpha_{23}],$$

$$L_{34} = D_{11}^s\alpha_{13} + (2D_{12}^s + 4D_{66}^s)\alpha_{11} + D_{22}^s\alpha_5$$
$$-\lambda[D_{11}^s\alpha_{22} + (2D_{12}^s + 4D_{66}^s + D_{11}^s)\alpha_{20} + (2D_{12}^s + 4D_{66}^s + D_{22}^s)\alpha_{21} + D_{22}^s\alpha_{23}]$$
$$-K_w\alpha_1 + K_g(\alpha_3 + \alpha_9) - \mu[-K_w\alpha_9 + K_g(\alpha_{11} + \alpha_{13}) - K_w\alpha_3 + K_g(\alpha_5 + \alpha_{11})],$$

$$L_{44} = H_{11}^s\alpha_{13} + (2H_{12}^s + 4H_{66}^s)\alpha_{11} + H_{22}^s\alpha_5 + J_{44}\alpha_9 + J_{55}\alpha_3$$
$$-\lambda[H_{11}^s\alpha_{22} + (2H_{12}^s + 4H_{66}^s + H_{11}^s)\alpha_{20} + J_{44}\alpha_{13} + (J_{55} + J_{44})\alpha_{11}$$
$$+(2H_{12}^s + 4H_{66}^s + H_{22}^s)\alpha_{21} + H_{22}^s\alpha_{23} + J_{55}\alpha_5] - K_w\alpha_1 + K_g(\alpha_3 + \alpha_9)$$
$$-\mu[-K_w\alpha_9 + K_g(\alpha_{11} + \alpha_{13}) - K_w\alpha_3 + K_g(\alpha_5 + \alpha_{11})], \tag{35}$$

$$(\alpha_1, \alpha_3, \alpha_5, \alpha_7, \alpha_9) = \int_0^b \int_0^a (X_m Y_n, X_m Y_n'', X_m Y_n'''', X_m' Y_n', X_m'' Y_n) \, X_m Y_n \mathrm{d}x\mathrm{d}y$$

$$(\alpha_2, \alpha_4, \alpha_{10}, \alpha_{17}, \alpha_{18}, \alpha_{19}) = \int_0^b \int_0^a (X_m Y_n', X_m Y_n''', X_m'' Y_n', X_m'''' Y_n', X_m'' Y_n''', X_m Y_n''''') \, X_m Y_n' \mathrm{d}x\mathrm{d}y$$

$$(\alpha_6, \alpha_8, \alpha_{12}, \alpha_{14}, \alpha_{15}, \alpha_{16}) = \int_0^b \int_0^a (X_m' Y_n, X_m' Y_n'', X_m''' Y_n, X_m''''' Y_n, X_m''' Y_n'', X_m' Y_n'''') \, X_m' Y_n \mathrm{d}x\mathrm{d}y$$

$$(\alpha_{11}, \alpha_{13}, \alpha_{20}, \alpha_{21}, \alpha_{22}, \alpha_{23}) = \int_0^b \int_0^a (X_m'' Y_n'', X_m'''' Y_n, X_m'''' Y_n'', X_m'' Y_n'''', X_m'''''' Y_n, X_m Y_n'''''') \, X_m Y_n \mathrm{d}x\mathrm{d}y \tag{36}$$

6. Numerical Results

In this section, the numerical outcomes are existing to demonstrate the static response of two models of FG sandwich nanoplates with simply supported boundary condision using the new higher-order shear deformation plate theory. The material selected for simulation is a mixture of aluminum (Al) and zirconia (ZrO₂). Young's modulus for aluminum are $E_m = 70\,\mathrm{GPa}$, and for zirconia are $E_c = 151\,\mathrm{GPa}$. Poisson's ratio is chosen as constant ($\nu_c = 0.3$). Numerical outcomes are offered in terms of non-dimensional stresses and deflection. The non-dimensional parameters are defined as

Dimensionless center deflection:

$$\bar{w} = \frac{10hE_0}{a^2 q_0} w\left(\frac{a}{2}, \frac{b}{2}\right), \tag{37}$$

Dimensionless axial stress:

$$\bar{\sigma}_{xx} = \frac{10h^2}{a^2 q_0} \sigma_{xx}\left(\frac{a}{2}, \frac{b}{2}, \frac{h}{2}\right), \tag{38}$$

Dimensionless shear stress:

$$\bar{\tau}_{xz} = \frac{h}{a q_0} \tau_{xz}\left(0, \frac{b}{2}, 0\right), \tag{39}$$

Foundation parameters:

$$k_w = \frac{a^4}{D} K_w, \quad k_g = \frac{a^2}{D} K_g, \tag{40}$$

where $D = \frac{h^3 E_c}{12(1-\nu^2)}$, and $E_0 = 1\,\mathrm{GPa}$ is the reference value. Different types of symmetric and non-symmetric FG sandwich plates are used [53, 54]:

The (1-1-1) FG sandwich plate: The plate is made of three equal-thickness layers:

$$h_1 = -\frac{h}{6}, \quad h_2 = \frac{h}{6}. \tag{41}$$

The (2-1-2) FG sandwich plate: The upper layer thickness is twice the core layer while it is the same as the lower one:

$$h_1 = -\frac{h}{10}, \quad h_2 = \frac{h}{10}. \tag{42}$$

The (2-2-1) FG sandwich plate: The core thickness is twice the upper face while it is the same as the lower one:

$$h_1 = -\frac{h}{10}, \quad h_2 = \frac{3h}{10}. \tag{43}$$

Table 1. Effects of volume fraction index on the dimensionless deflection, dimensionless axial stress and dimensionless shear stress of simply supported P-FGSP sandwich plates.

Theory	p	1-1-1			2-1-2			2-2-1		
		$\bar{w}$	$\bar{\sigma}_{xx}$	$\bar{\tau}_{xz}$	$\bar{w}$	$\bar{\sigma}_{xx}$	$\bar{\tau}_{xz}$	$\bar{w}$	$\bar{\sigma}_{xx}$	$\bar{\tau}_{xz}$
SSDT [3]	0	0.19605	2.05452	0.24618	0.19605	2.05452	0.24618	0.19605	2.05452	0.24618
TSDT [3]		0.19606	2.04985	0.23857	0.19606	2.04985	0.23857	0.19606	2.04985	0.23857
5SDT		0.19456	1.98728	0.20180	0.19456	1.98728	0.20180	0.19456	1.98728	0.20180
7SDT		0.19572	2.05355	0.28134	0.19572	2.05355	0.28134	0.19572	2.05355	0.28134
Present		0.19605	2.04610	0.23252	0.19606	2.04610	0.23252	0.19605	2.04610	0.23252
SSDT [3]	1	0.29194	1.42892	0.26809	0.30624	1.49859	0.27774	0.28082	1.32342	0.26680
TSDT [3]		0.29199	1.42617	0.26117	0.30632	1.49587	0.27104	0.28085	1.32062	0.25951
5SDT		0.29111	1.39225	0.24121	0.30539	1.46096	0.24968	0.27991	1.28648	0.24968
7SDT		0.29157	1.42937	0.30402	0.30574	1.49856	0.31196	0.28046	1.32370	0.31196
Present		0.29201	1.42396	0.25565	0.30635	1.49368	0.26566	0.28085	1.31838	0.25371
SSDT [3]	2	0.33280	1.63025	0.27807	0.35218	1.72412	0.29422	0.31611	1.47387	0.27627
TSDT [3]		0.33289	1.62748	0.27188	0.35231	1.72144	0.28838	0.31617	1.47095	0.26939
5SDT		0.33213	1.59267	0.25416	0.35144	1.68504	0.26740	0.31534	1.43551	0.25064
7SDT		0.33232	1.63083	0.31227	0.35147	1.72368	0.32518	0.31569	1.47437	0.31212
Present		0.33293	1.62525	0.26690	0.35239	1.71926	0.28361	0.31619	1.46860	0.26390
SSDT [3]	5	0.37128	1.81838	0.29150	0.39160	1.91547	0.31930	0.34950	1.61477	0.28895
TSDT [3]		0.37145	1.81580	0.28643	0.39183	1.91302	0.31454	0.34960	1.61181	0.28265
5SDT		0.37069	1.78025	0.26752	0.39081	1.87455	0.28869	0.34880	1.57515	0.26366
7SDT		0.37056	1.81826	0.32096	0.39047	1.91346	0.34357	0.34892	1.61514	0.32262
Present		0.37155	1.81370	0.28226	0.39197	1.91099	0.31050	0.34966	1.60943	0.27757
SSDT [3]	10	0.38490	1.88147	0.29529	0.40376	1.97313	0.33644	0.34916	1.61979	0.29671
TSDT [3]		0.38551	1.88376	0.29566	0.40407	1.97126	0.33242	0.36215	1.66660	0.29080
5SDT		0.38469	1.84756	0.27460	0.40287	1.93099	0.30181	0.36129	1.62737	0.27061
7SDT		0.38439	1.88529	0.32614	0.40241	1.97042	0.35759	0.36132	1.66795	0.32936
Present		0.38565	1.88177	0.29188	0.40425	1.96929	0.32849	0.36220	1.66240	0.28588

Table 2. Effects of nonlocal and length scale parameters on dimensionless deflection, dimensionless axial stress and dimensionless shear stress of P-FGSP sandwich nanoplates.

BC	μ	λ	1-1-1			2-1-2			2-2-1		
			$\bar{w}$	$\bar{\sigma}_{xx}$	$\bar{\tau}_{xz}$	$\bar{w}$	$\bar{\sigma}_{xx}$	$\bar{\tau}_{xz}$	$\bar{w}$	$\bar{\sigma}_{xx}$	$\bar{\tau}_{xz}$
SSSS	0	0	0.3329	1.4867	0.8654	0.3523	1.5731	0.9179	0.3162	1.1671	0.8575
		1	0.2780	1.2416	0.7227	0.2942	1.3138	0.7666	0.2640	0.9747	0.7161
		2	0.2387	1.0659	0.6205	0.2526	1.1278	0.6581	0.2267	0.8367	0.6148
	1	0	0.3986	1.7801	1.0362	0.4219	1.8836	1.0991	0.3786	1.3974	1.0268
		1	0.3329	1.4867	0.8654	0.3523	1.5731	0.9179	0.3162	1.1671	0.8575
		2	0.2858	1.2763	0.7429	0.3025	1.3505	0.7880	0.2714	1.0019	0.7361
	2	0	0.4643	2.0736	1.2071	0.4914	2.1941	1.2803	0.4410	1.6278	1.1960
		1	0.3878	1.7318	1.0081	0.4104	1.8324	1.0693	0.3683	1.3595	0.9989
		2	0.3329	1.4867	0.8654	0.3523	1.5731	0.9179	0.3162	1.1671	0.8575
CCCC	0	0	0.1766	0.6637	1.1529	0.1869	0.7017	1.2229	0.1682	0.5052	1.1424
		1	0.1114	0.4134	0.7553	0.1178	0.4371	0.8012	0.1061	0.3139	0.7484
		2	0.0813	0.3001	0.5616	0.0861	0.3173	0.5957	0.0775	0.2276	0.5565
	1	0	0.2115	0.7947	1.3805	0.2238	0.8403	1.4643	0.2014	0.6049	1.3679
		1	0.1333	0.4950	0.9044	0.1411	0.5234	0.9593	0.1270	0.3759	0.8961
		2	0.0974	0.3593	0.6725	0.1030	0.3799	0.7133	0.0928	0.2725	0.6663
	2	0	0.2463	0.9257	1.6081	0.2607	0.9788	1.7057	0.2346	0.7046	1.5934
		1	0.1553	0.5766	1.0535	0.1644	0.6096	1.1174	0.1479	0.4378	1.0439
		2	0.1134	0.4186	0.7833	0.1200	0.4425	0.8309	0.1080	0.3174	0.7762
CSCS	0	0	0.2056	0.8125	1.2731	0.2175	0.8593	1.3504	0.1956	0.6245	1.2611
		1	0.1407	0.5541	0.8706	0.1489	0.5860	0.9235	0.1339	0.4256	0.8625
		2	0.1069	0.4202	0.6615	0.1132	0.4444	0.7017	0.1018	0.3226	0.6553
	1	0	0.2461	0.9729	1.5244	0.2605	1.0290	1.6169	0.2342	0.7477	1.5100
		1	0.1684	0.6634	1.0425	0.1782	0.7016	1.1058	0.1603	0.5096	1.0327
		2	0.1280	0.5031	0.7921	0.1355	0.5321	0.8402	0.1218	0.3863	0.7847
	2	0	0.2867	1.1333	1.7757	0.3034	1.1986	1.8835	0.2728	0.8710	1.7590
		1	0.1962	0.7728	1.2143	0.2076	0.8173	1.2880	0.1867	0.5936	1.2029
		2	0.1491	0.5860	0.9227	0.1578	0.6198	0.9787	0.1419	0.4499	0.9141
CCSS	0	0	0.0675	0.2705	0.3460	0.0714	0.2861	0.3670	0.0642	0.2084	0.3428
		1	0.0454	0.1795	0.2463	0.0480	0.1898	0.2613	0.0432	0.1380	0.2440
		2	0.0342	0.1342	0.1912	0.0362	0.1420	0.2028	0.0325	0.1031	0.1895
	1	0	0.0808	0.3239	0.4143	0.0855	0.3426	0.4394	0.0768	0.2496	0.4105
		1	0.0543	0.2149	0.2949	0.0575	0.2273	0.3128	0.0517	0.1652	0.2922
		2	0.0409	0.1607	0.2290	0.0433	0.1700	0.2428	0.0390	0.1234	0.2269
	2	0	0.0941	0.3773	0.4826	0.0996	0.3990	0.5119	0.0895	0.2907	0.4782
		1	0.0633	0.2504	0.3435	0.0670	0.2648	0.3644	0.0602	0.1925	0.3404
		2	0.0477	0.1872	0.2667	0.0505	0.1980	0.2829	0.0454	0.1437	0.2643

Similar theories of the five- (5SDT) and seven-order (7SDT) shear deformation are given by Nguyen-Xuan et al. [55] and Nguyen et al. [56], respectively. The 5SDT [55] is considered by setting $\Psi(z) = \frac{7}{8}z - \frac{2}{h^2}z^3 + \frac{2}{h^4}z^5$ while the 7SDT [56] is considered by setting $\Psi(z) = z - \frac{87}{20h^2}z^3 + \frac{169}{10h^4}z^5 + \frac{138}{5h^6}z^7$. Both theories are used in this research to evaluate the accuracy and reliability of the proposed theory.
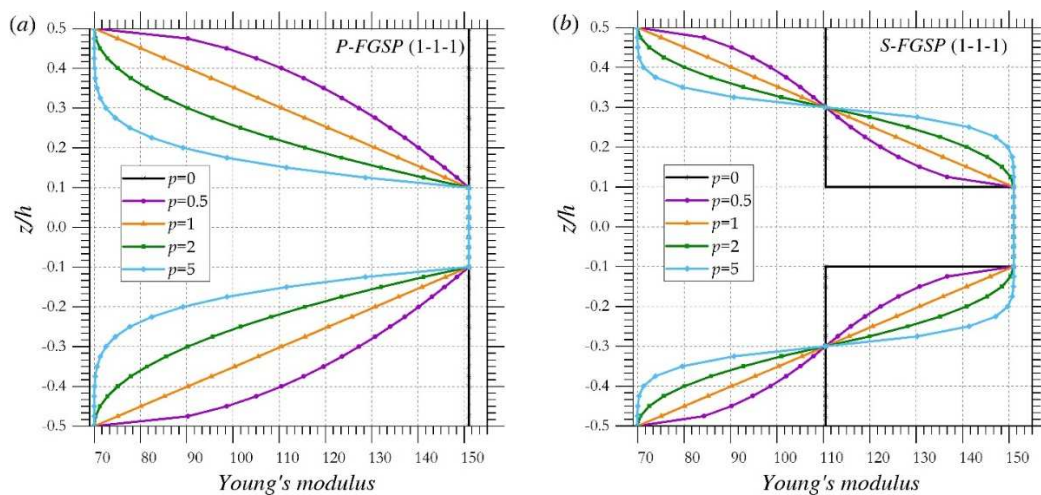
Fig. 2. Variation of Young's modulus through FG sandwich plate thickness.

Table 1 illustrates the effects of volume fraction index on the dimensionless deflection, dimensionless axial stress, and dimensionless shear stress of P-FGSP for different sandwich schemes by using different higher-order shear deformation theories. Clearly, the present theory is in close agreement with those generated by Zenkour [3], and particularly the third-order shear deformation theory.

In Tables 2 and 3, we present the effects of nonlocal and length scale parameters on the dimensionless deflection, dimensionless axial stress, and dimensionless shear stress of square P-FGSP and S-FGSP under various boundary conditions. The impact of volume fraction p, elastic foundation parameters, and various boundary conditions on the dimensionless deflection of P-FGSP and S-FGSP sandwich plates (1-1-1) is presented in Table 4 for nonlocal and length scale parameters $\lambda = \mu = 1$ and side to thickness $a/h = 10$.

Table 3. Effects of nonlocal and length scale parameters on dimensionless deflection, dimensionless axial stress and dimensionless shear stress of S-FGSP sandwich nanoplates.

BC	μ	λ	1-1-1			2-1-2			2-2-1		
			$\bar{w}$	$\bar{\sigma}_{xx}$	$\bar{\tau}_{xz}$	$\bar{w}$	$\bar{\sigma}_{xx}$	$\bar{\tau}_{xz}$	$\bar{w}$	$\bar{\sigma}_{xx}$	$\bar{\tau}_{xz}$
SSSS	0	0	0.3006	1.3348	0.8247	0.3187	1.4196	0.8498	0.2880	1.0929	0.8200
		1	0.2511	1.1148	0.6888	0.2662	1.1855	0.7097	0.2405	0.9128	0.6848
		2	0.2155	0.9570	0.5913	0.2285	1.0178	0.6092	0.2065	0.7836	0.5879
	1	0	0.3600	1.5983	0.9875	0.3816	1.6998	1.0175	0.3448	1.3087	0.9819
		1	0.3006	1.3348	0.8247	0.3187	1.4196	0.8498	0.2880	1.0929	0.8200
		2	0.2581	1.1459	0.7080	0.2736	1.2187	0.7295	0.2472	0.9383	0.7040
	2	0	0.4193	1.8618	1.1503	0.4445	1.9800	1.1852	0.4016	1.5244	1.1438
		1	0.3502	1.5549	0.9607	0.3713	1.6536	0.9898	0.3354	1.2731	0.9552
		2	0.3006	1.3348	0.8247	0.3187	1.4196	0.8498	0.2880	1.0929	0.8200
CCCC	0	0	0.1601	0.5917	1.0987	0.1694	0.6316	1.1321	0.1536	0.4713	1.0925
		1	0.1009	0.3684	0.7198	0.1068	0.3933	0.7417	0.0969	0.2927	0.7157
		2	0.0737	0.2673	0.5352	0.0780	0.2855	0.5515	0.0708	0.2122	0.5322
	1	0	0.1916	0.7085	1.3156	0.2028	0.7563	1.3556	0.1840	0.5643	1.3081
		1	0.1209	0.4411	0.8619	0.1279	0.4710	0.8880	0.1161	0.3505	0.8570
		2	0.0883	0.3201	0.6408	0.0934	0.3419	0.6603	0.0848	0.2541	0.6372
	2	0	0.2232	0.8253	1.5325	0.2362	0.8810	1.5790	0.2143	0.6573	1.5238
		1	0.1408	0.5138	1.0039	0.1490	0.5486	1.0344	0.1352	0.4083	0.9982
		2	0.1028	0.3729	0.7465	0.1088	0.3982	0.7692	0.0987	0.2960	0.7423
CSCS	0	0	0.1861	0.7260	1.2127	0.1970	0.7741	1.2498	0.1785	0.5833	1.2056
		1	0.1274	0.4950	0.8294	0.1348	0.5278	0.8548	0.1222	0.3975	0.8245
		2	0.0968	0.3753	0.6302	0.1025	0.4003	0.6495	0.0929	0.3013	0.6266
	1	0	0.2228	0.8693	1.4521	0.2359	0.9269	1.4966	0.2138	0.6984	1.4435
		1	0.1525	0.5927	0.9931	0.1615	0.6320	1.0235	0.1463	0.4759	0.9873
		2	0.1159	0.4494	0.7546	0.1227	0.4793	0.7777	0.1112	0.3607	0.7502
	2	0	0.2596	1.0126	1.6915	0.2748	1.0797	1.7433	0.2490	0.8135	1.6815
		1	0.1776	0.6904	1.1569	0.1881	0.7362	1.1922	0.1704	0.5544	1.1501
		2	0.1350	0.5235	0.8790	0.1430	0.5583	0.9059	0.1296	0.4202	0.8739
CCSS	0	0	0.0611	0.2418	0.3297	0.0646	0.2578	0.3397	0.0586	0.1948	0.3278
		1	0.0411	0.1604	0.2347	0.0435	0.1710	0.2418	0.0394	0.1289	0.2334
		2	0.0310	0.1199	0.1822	0.0328	0.1279	0.1878	0.0297	0.0962	0.1812
	1	0	0.0731	0.2896	0.3948	0.0774	0.3087	0.4068	0.0701	0.2332	0.3926
		1	0.0492	0.1921	0.2810	0.0521	0.2048	0.2896	0.0472	0.1543	0.2795
		2	0.0371	0.1436	0.2182	0.0392	0.1531	0.2248	0.0356	0.1152	0.2169
	2	0	0.0852	0.3373	0.4599	0.0902	0.3595	0.4739	0.0817	0.2717	0.4573
		1	0.0573	0.2237	0.3274	0.0607	0.2385	0.3373	0.0550	0.1798	0.3255
		2	0.0432	0.1673	0.2542	0.0457	0.1784	0.2619	0.0414	0.1342	0.2527

Table 4. Effects of elastic foundation parameters and various boundary conditions on dimensionless deflection of FGSP sandwich nanoplate (1-1-1).

|	BC	p	$K_w = 0$			$K_w = 50$			$K_w = 100$		
			$K_g = 0$	$K_g = 50$	$K_g = 100$	$K_g = 0$	$K_g = 50$	$K_g = 100$	$K_g = 0$	$K_g = 50$	$K_g = 100$
P-FGSP	SSSS	0	0.1961	0.0533	0.0309	0.1727	0.0514	0.0302	0.1542	0.0497	0.0296
		1	0.2920	0.0586	0.0326	0.2429	0.0563	0.0318	0.2080	0.0542	0.0312
		2	0.3329	0.0601	0.0330	0.2706	0.0577	0.0323	0.2280	0.0554	0.0316
		5	0.3714	0.0612	0.0333	0.2955	0.0587	0.0326	0.2454	0.0564	0.0319
	CCCC	0	0.0807	0.0393	0.0260	0.0781	0.0387	0.0257	0.0757	0.0381	0.0254
		1	0.1176	0.0464	0.0289	0.1122	0.0455	0.0286	0.1073	0.0447	0.0282
		2	0.1333	0.0487	0.0298	0.1264	0.0477	0.0294	0.1202	0.0468	0.0291
		5	0.1482	0.0505	0.0304	0.1397	0.0495	0.0301	0.1322	0.0485	0.0297
	CSCS	0	0.1011	0.0423	0.0267	0.0959	0.0413	0.0263	0.0913	0.0404	0.0260
		1	0.1483	0.0488	0.0292	0.1375	0.0475	0.0287	0.1281	0.0463	0.0283
		2	0.1684	0.0507	0.0299	0.1546	0.0494	0.0294	0.1428	0.0481	0.0290
		5	0.1875	0.0523	0.0304	0.1704	0.0509	0.0299	0.1563	0.0496	0.0295
	CCSS	0	0.0326	0.0141	0.0090	0.0314	0.0139	0.0089	0.0303	0.0137	0.0088
		1	0.0478	0.0164	0.0099	0.0453	0.0161	0.0098	0.0430	0.0158	0.0097
		2	0.0543	0.0171	0.0102	0.0510	0.0168	0.0100	0.0481	0.0164	0.0099
		5	0.0605	0.0177	0.0104	0.0564	0.0173	0.0102	0.0529	0.0170	0.0101
S-FGSP	SSSS	0	0.2621	0.0573	0.0321	0.2219	0.0551	0.0314	0.1924	0.0531	0.0308
		1	0.2920	0.0586	0.0326	0.2429	0.0563	0.0318	0.2080	0.0542	0.0312
		2	0.3006	0.0589	0.0327	0.2489	0.0566	0.0319	0.2124	0.0545	0.0312
		5	0.3071	0.0592	0.0327	0.2533	0.0568	0.0320	0.2156	0.0547	0.0313
	CCCC	0	0.1065	0.0446	0.0282	0.1020	0.0438	0.0279	0.0979	0.0430	0.0275
		1	0.1176	0.0464	0.0289	0.1122	0.0455	0.0286	0.1073	0.0447	0.0282
		2	0.1209	0.0469	0.0291	0.1152	0.0460	0.0288	0.1100	0.0452	0.0284
		5	0.1233	0.0473	0.0292	0.1174	0.0464	0.0289	0.1120	0.0455	0.0285
	CSCS	0	0.1339	0.0471	0.0286	0.1250	0.0459	0.0281	0.1172	0.0448	0.0277
		1	0.1483	0.0488	0.0292	0.1375	0.0475	0.0287	0.1281	0.0463	0.0283
		2	0.1525	0.0492	0.0293	0.1410	0.0479	0.0289	0.1312	0.0467	0.0284
		5	0.1556	0.0495	0.0294	0.1437	0.0482	0.0290	0.1335	0.0470	0.0285
	CCSS	0	0.0432	0.0158	0.0097	0.0411	0.0155	0.0096	0.0392	0.0153	0.0095
		1	0.0478	0.0164	0.0099	0.0453	0.0161	0.0098	0.0430	0.0158	0.0097
		2	0.0492	0.0166	0.0100	0.0465	0.0162	0.0098	0.0440	0.0159	0.0097
		5	0.0502	0.0167	0.0100	0.0474	0.0164	0.0099	0.0449	0.0160	0.0098
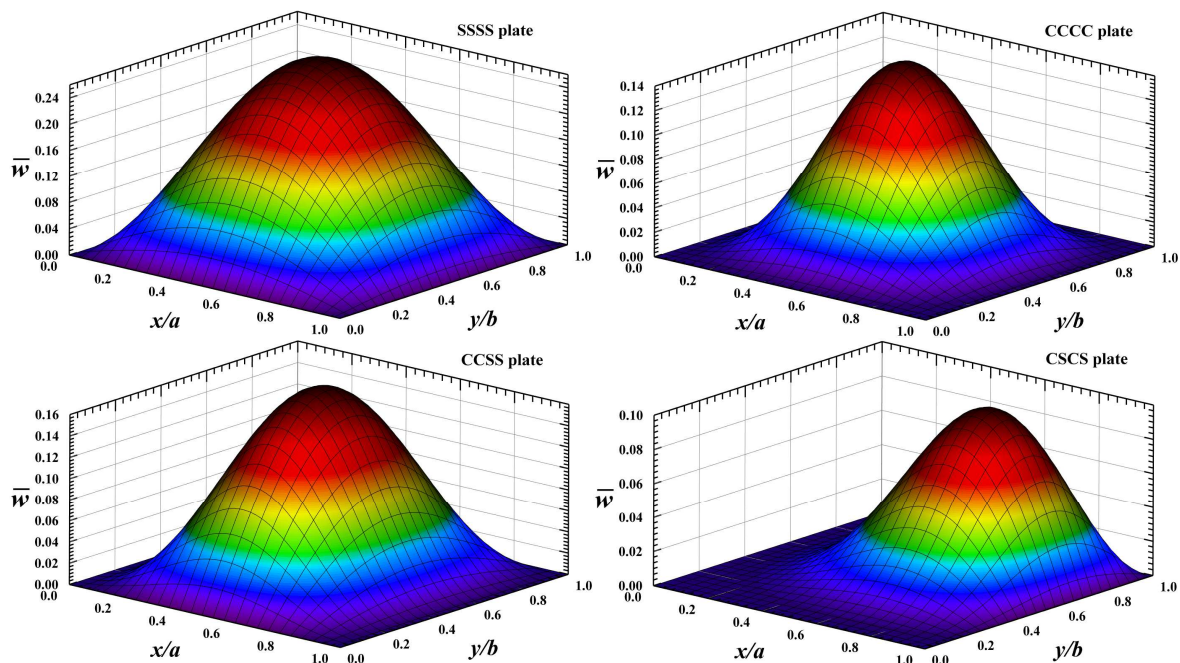
Fig. 3. Dimensionless center deflection of P-FGSP (1-1-1) with various boundary conditions $(p = 1, a/h = 10)$.

Figure 2 presents variation of volume fraction of P-FGSP and S-FGSP sandwich plates using the different schemes. From this figure, the volume fraction of P-FGSP sandwich plates have smooth variation in the interfaces just for the values of index $p < 1$. When the volume index decreases more, the quantity of ceramic increases. This can limit the performance of the sandwich structure. Therefore, we present another model of FG sandwich structure depending on the sigmoid capacity. As can be seen, the volume fraction of S-FGSPs for index $p > 1$ has an ideal distribution in the interfaces. Additionally, the ceramic has half of the volume of each FG layer while the remaining half is metal any place the volume part list is.
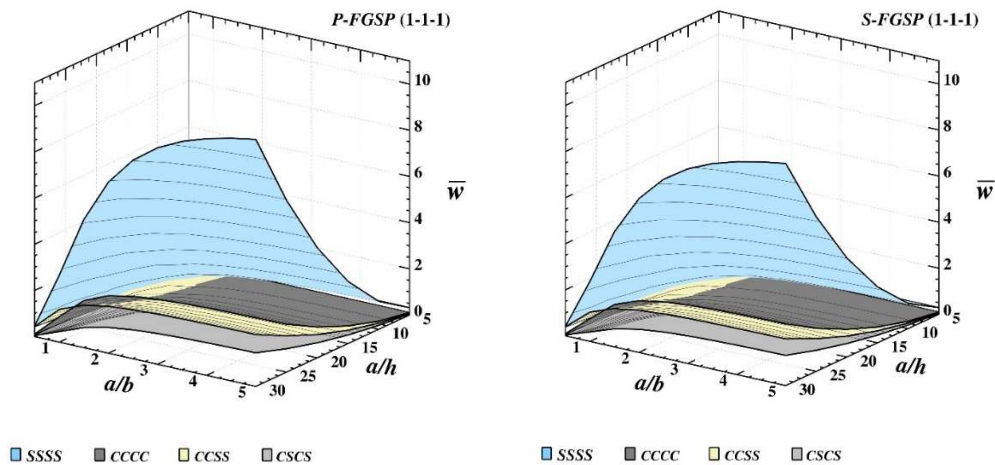
Fig. 4. Dimensionless center deflection of square FG sandwich plate (1-1-1) versus side to thickness and aspect ratio parameters $(p = 2, \mu = \lambda = 1)$.
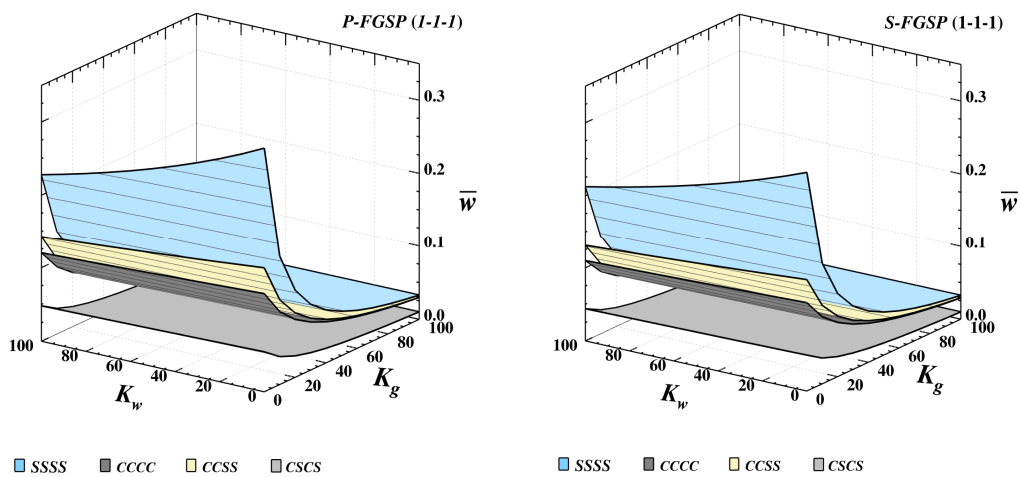

Fig. 5. Dimensionless center deflection of square FG sandwich plate (1-1-1) versus two elastic foundation parameters $(p = 2, a/h = 10, \lambda = \mu = 1)$.
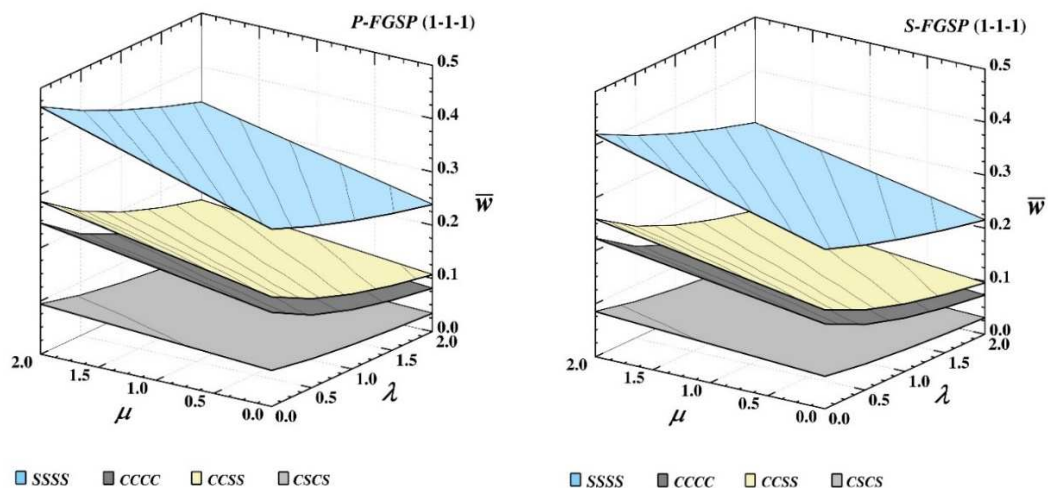

Fig. 6. Dimensionless center deflection of square FG sandwich plate (1-1-1) versus nonlocal parameter and length scale parameter $(p = 2, a/h = 10)$.

In figures 3, the dimensionless center deflection of P-FGSP under various boundary conditions is illustrated. The maximum deflections are for the simply supported SSSS nanoplates, and the minimum deflections are for the CSCS plates.

The effect of side-to-thickness a/h and aspect ratio b/a on the dimensionless deflection of P-FGSP and S-FGSP sandwich plates for various boundary conditions are presented in Figure 4. The dimensionless deflection increases as side to thickness and aspect ratio increases regardless of the boundary conditions and FGM type. The deflection of the simply supported SSSS sandwich nanoplates is found to be of the largest, while the CSCS sandwich nanoplates have the smallest deflections.
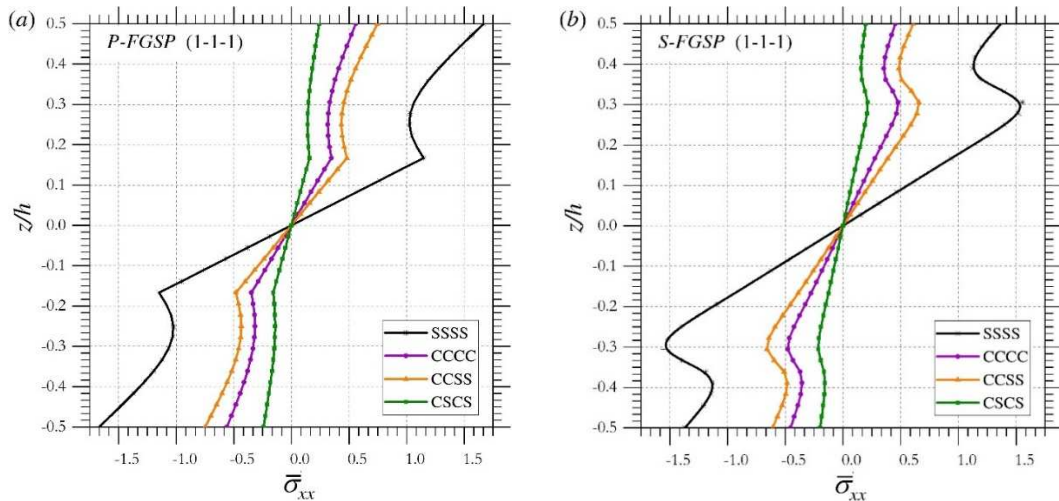
Fig. 7. Dimensionless axial stress through-the-thickness of square FG sandwich plate with various boundary conditions $(p = 5, \mu = \lambda = 1)$.
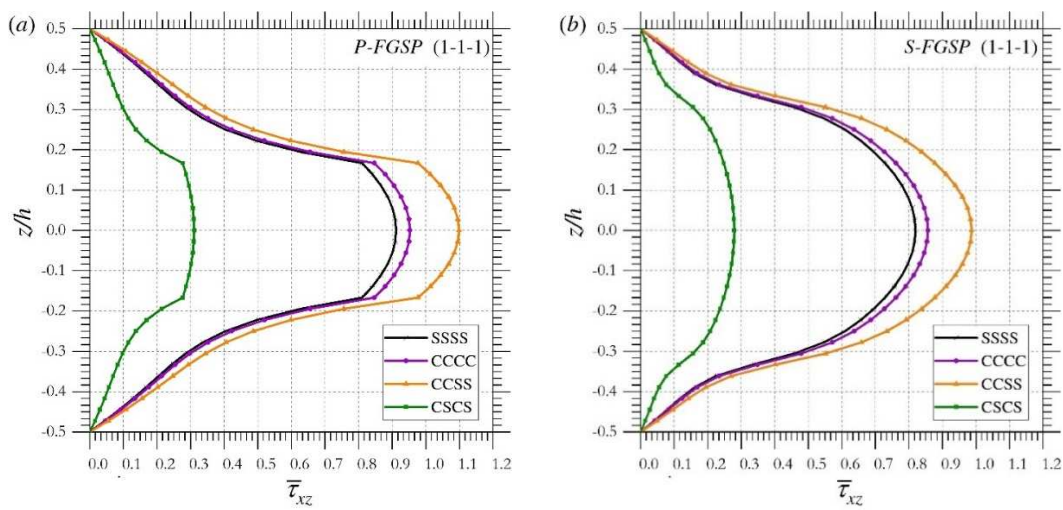
Fig. 8. Dimensionless shear stress through-the-thickness of square FG sandwich plate with various boundary conditions $(p = 5, a/h = 10, \mu = \lambda = 1)$.
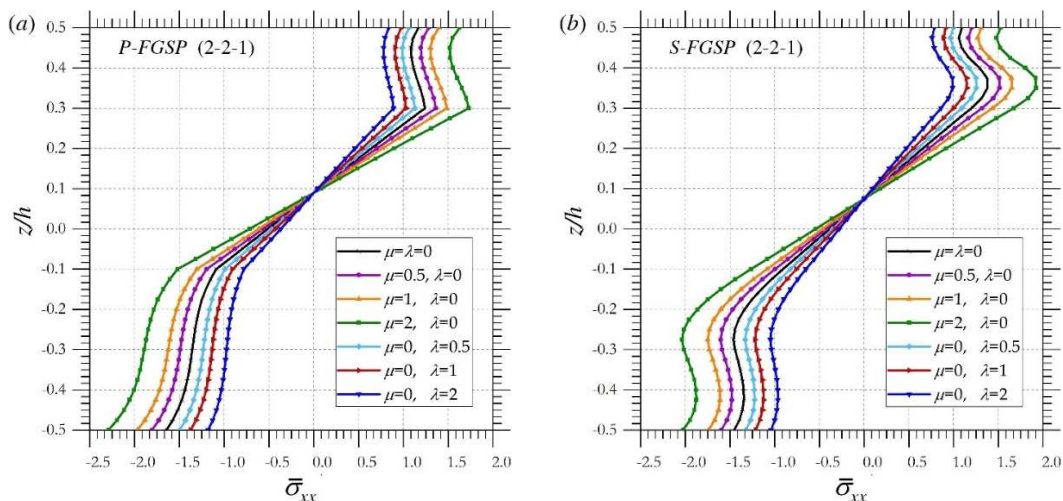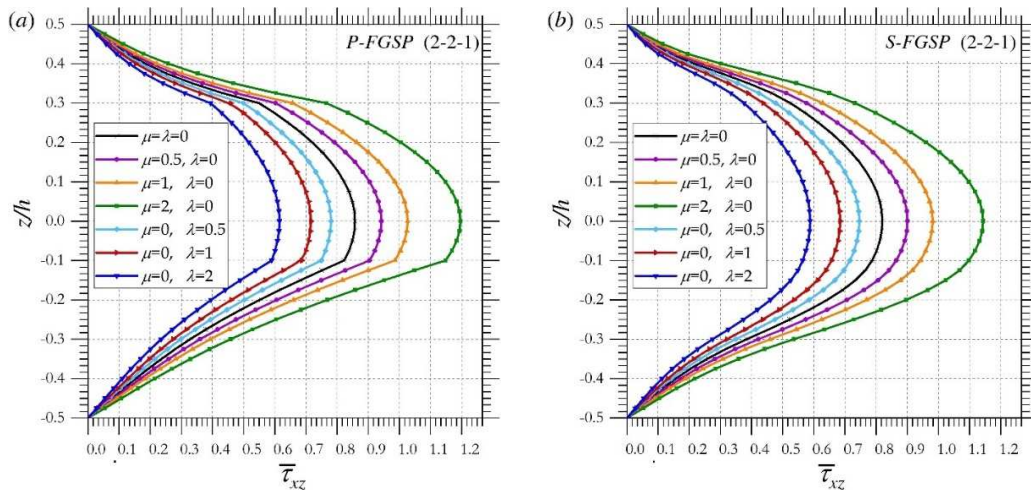

Fig. 9. Dimensionless axial stress through-the-thickness of simply supported square FG sandwich plate $(p = 2, a/h = 10)$.

The impact of elastic foundation parameters K_w and K_g on the dimensionless central deflection of P-FGSP and S-FGSP is plotted in Figure 5. The increase of these parameters leads to decrement of transverse deflection $\bar{w}$. It can be seen that the Pasternak foundation parameter K_g has more effect than the Winkler foundation K_w parameter on increasing the nondimensional frequency.

In Figure 6, we presented the influence of length scale parameter and nonlocal parameter on the dimensionless center deflection of square FG sandwich nanoplate with various boundary conditions. It can be observed that the increase of length scale parameter λ lead to decrement of transverse displacement, while transverse displacement increases by increasing of nonlocal parameter μ wherever the sandwich type and boundary condition is. therefore, we can conclude that the inclusion of size effects reduces of the stiffness of the FG sandwich nanoplates.

Fig. 10. Dimensionless shear stress through-the-thickness of simply supported square FG sandwich plate $(p = 2, a/h = 10)$.
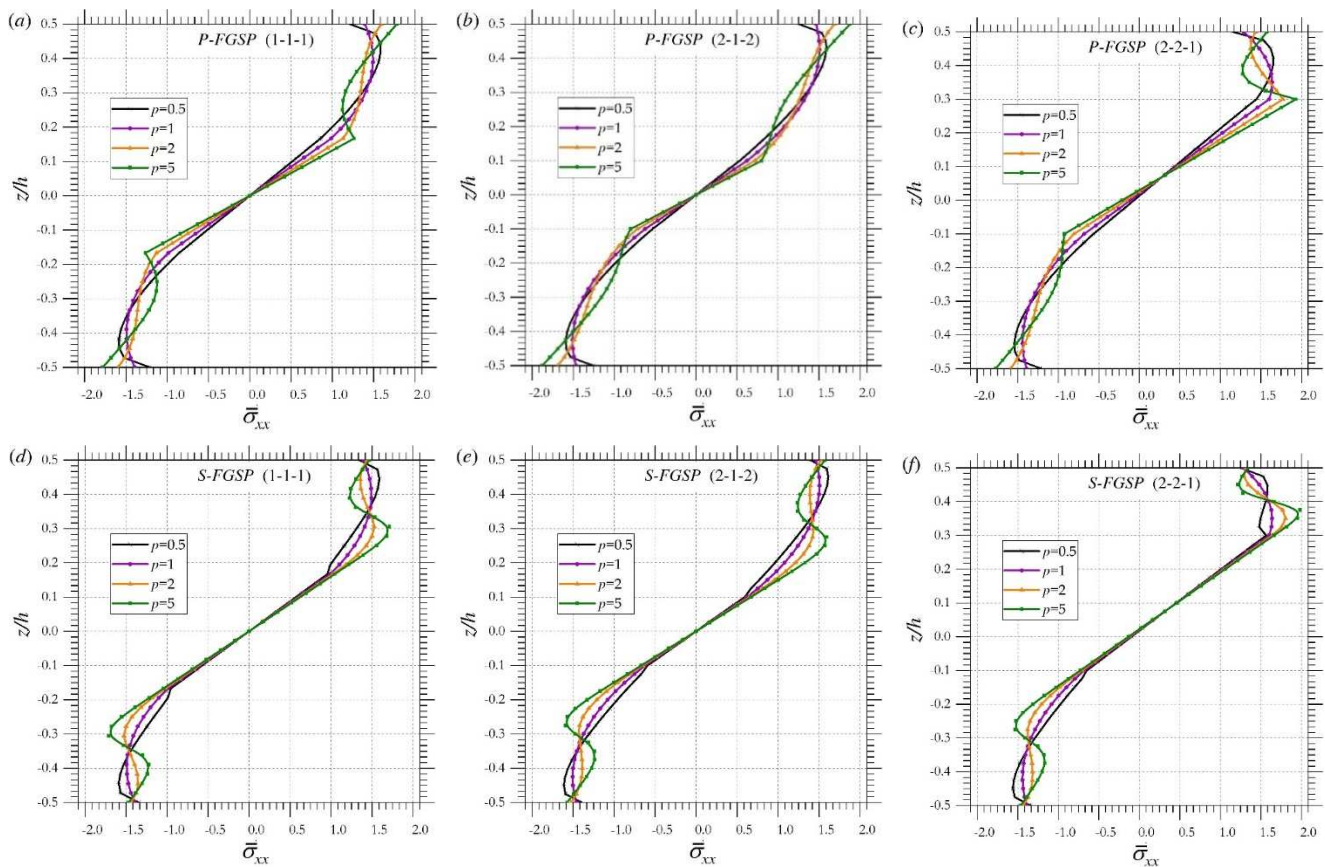

Fig. 11. Dimensionless axial stress through-the-thickness of FG sandwich plate.

Figures 7 and 8 shows dimensionless axial stresses $\bar{\sigma}_{xx}$ and shear stresses $\bar{\tau}_{xx}$ distributions through the nanoplate thickness, respectively, using various boundary conditions. The maximum values of axial stresses $\bar{\sigma}_{xx}$ are for the simply supported SSSS nanoplates, and the minimum values are for the CSCS plates, while, for the shear stresses $\bar{\tau}_{xx}$ case, The maximum values are for the CCSS nanoplates and the minimum values are for CSCS nanoplates.

To have a better understanding of the nonlocal and length scale parameters effect, variations of dimensionless axial stresses $\bar{\sigma}_{xx}$ and shear stresses $\bar{\tau}_{xx}$ across the thickness direction of simply supported P-FGSP and S-FGSP have been plotted in figures 9 and 10 respectively. As can be seen, the dimensionless axial stresses $\bar{\sigma}_{xx}$ and shear stresses $\bar{\tau}_{xx}$ increase by increasing of nonlocal parameter μ or decreasing of length scale parameters λ. The dimensional axial stress thought the sandwich nanoplate thickness with simply supported boundary condition and for different value of index p is presented in Figure 11. The stresses are tensile at the top surface and compressive at the bottom surface. The FG nanoplate for $p = 5$ yields the maximum compressive (tensile) stress at the bottom (top) surface. In Figure 12, the dimensional shear stress thought the sandwich nanoplate thickness for different value of index p is illustrated. The maximum value occurs at a point on the mid-plane of the sandwich nanoplate. In the case of P-FGSPs, the largest magnitude is obtained for $p = 5$. However, for S-FGSPs, the largest magnitude is for $p = 0.5$. It is found that the dimensionless shear stress is continuous and smooth through the S-FGSP thickness regardless of the volume fraction index.

Figure 13 shows the variation of the dimensionless deflection with the volume fraction exponent p for the for different sandwich nanoplate schemes. The dimensionless deflection of S-FGSPs is larger than of P-FGSPs for index $p \leq 1$, and smaller for $p \geq 1$. In general, the dimensionless deflection increases as p rises and as the core thickness, with respect to the total thickness of the nanoplate, decreases.
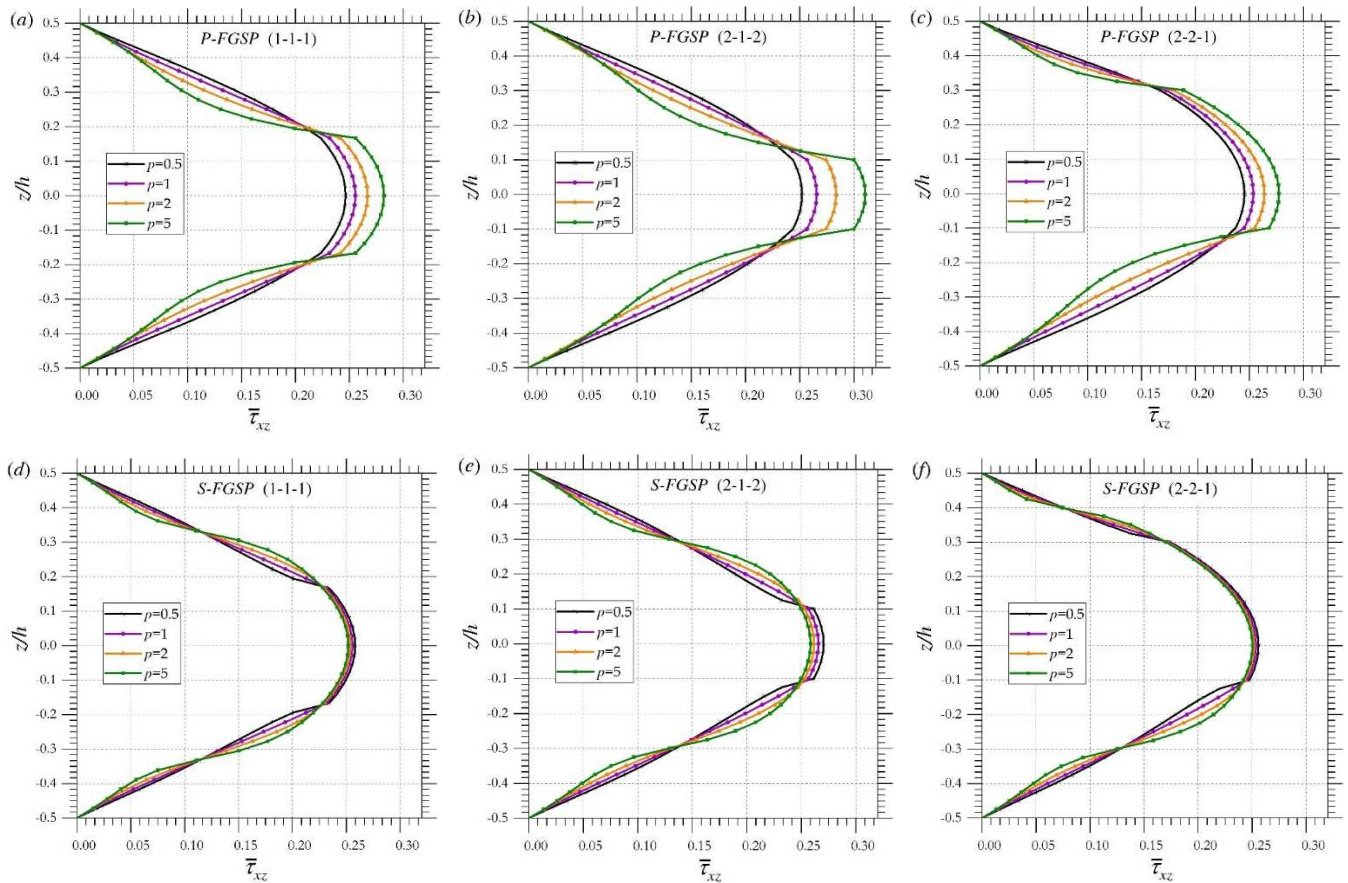
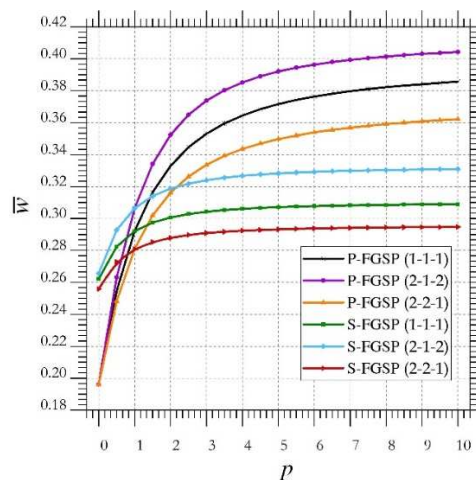**Fig. 12.** Dimensionless shear stress through-the-thickness of FG sandwich plate.

Fig. 13. Dimensionless deflection as a function of the volume fraction index.

7. Conclusions

In this study, an analytical solution for bending of new form functionally graded sandwich nanoplates resting on elastic foundation is presented. The method is based on a new higher-order shear deformation and nonlocal strain gradient theory considering various boundary conditions. Material properties of FG face layers are assumed to vary continuously through-the-thickness according to a simple power-law distribution or sigmoid function distribution in terms of the volume fractions of the constituents. The governing equations of FG nanoplates have been derived based on higher-order deformation theory. Analytical solutions for FG sandwich nanoplates are developed for different boundary conditions. As a result, the dimensionless deflection increases as the side-to-thickness ratio rises. The inhomogeneity parameter plays a significant role in determining the response of the FG nanoplates. A fair agreement is obtained between the present results and those given from the literature. Pasternak foundation parameter has more effect on increasing dimensionless deflection than the Winkler parameter. Furthermore, the increase of nonlocality and strain gradient size-dependency leads to decrement and increment the stiffness of the FG sandwich nanoplate, respectively. It means that the axial and shear stresses amplified by increasing nonlocal parameter while the length scale parameter decreased the stresses. In addition to its excellent material properties, S-FGSPs predict good results for mechanical bending response.

Author Contributions

A.A. Daikh planned the scheme, initiated the problem and suggested the method of solution; A.M. Zenkour obtained the governing equations; analyzed the empirical results; the two authors developed the mathematical modeling and examined the theory validation. The manuscript was written through the contribution of the two authors. They discussed the results, reviewed, and approved the final version of the article.

Conflict of Interest

The authors declared no potential conflicts of interest with respect to the research, authorship, and publication of this article.

Funding

The authors received no financial support for the research, authorship, and publication of this article.

References

[1] Miyamoto, Y., Kaysser, W., Rabin, B., Kawasaki, A., Ford, R.G., *Functionally graded materials: design, processing and applications*, Springer Science & Business Media, 1999.
[2] Finot, M., Suresh, S., Bull, C., Sampath, S., Curvature changes during thermal cycling of a compositionally graded Ni/A12O3 multi-layered material, *Materials Science and Engineering: A*, 205 1996, 59-71.
[3] Zenkour, A.M., A comprehensive analysis of functionally graded sandwich plates: Part 1—Deflection and stresses, *International Journal of Solids and Structures*, 42, 2005, 5224-5242.
[4] Zenkour, A.M., The effect of transverse shear and normal deformations on the thermomechanical bending of functionally graded sandwich plates, *International Journal of Applied Mechanics*, 1, 2009, 667-707.
[5] Wang, Z.X., Shen, H.S., Nonlinear analysis of sandwich plates with FGM face sheets resting on elastic foundations, *Composite Structures*, 93, 2011, 2521-2532.
[6] Zenkour, A.M., Alghamdi, N., Thermoelastic bending analysis of functionally graded sandwich plates, *Journal of Materials Science*, 43, 2008, 2574-2589.
[7] Zenkour, A.M., Alghamdi, N., Bending analysis of functionally graded sandwich plates under the effect of mechanical and thermal loads, *Mechanics of Advanced Materials and Structures*, 17, 2010, 419-432.
[8] Zenkour, A.M., Alghamdi, N., Thermomechanical bending response of functionally graded nonsymmetric sandwich plates, *Journal of Sandwich Structures & Materials*, 12, 2010, 7-46.
[9] Merdaci, S., Tounsi, A., Houari, M.S.A., Mechab, I., Hebali, H., Benyoucef, S., Two new refined shear displacement models for functionally graded sandwich plates, *Archive of Applied Mechanics*, 51, 2011, 1507-1522.
[10] Natarajan, S., Manickam, G., Bending and vibration of functionally graded material sandwich plates using an accurate theory, *Finite Elements in Analysis and Design*, 57, 2012, 32-42.
[11] Iurlaro, L., Gherlone, M., Di Sciuva, M., Bending and free vibration analysis of functionally graded sandwich plates using the refined zigzag theory, *Journal of Sandwich Structures & Materials*, 16, 2014, 669-699.
[12] Thai, H-T., Nguyen, T-K., Vo, T. P., Lee, J., Analysis of functionally graded sandwich plates using a new first-order shear deformation theory, *European Journal of Mechanics-A/Solids*, 45, 2014, 211-225.
[13] Mahi, A., El Abbas, A.B., Tounsi, A., A new hyperbolic shear deformation theory for bending and free vibration analysis of isotropic, functionally graded, sandwich and laminated composite plates, *Applied Mathmatical Modelling*, 39, 2015, 2489-2508.
[14] Mantari, J., Granados, E., A refined FSDT for the static analysis of functionally graded sandwich plates, *Thin-Walled Structures*, 90, 2015, 150-158.
[15] Nguyen, T-K., Nguyen, V-H., Chau-Dinh, T., Vo, T. P., Nguyen-Xuan, H., Static and vibration analysis of isotropic and functionally graded sandwich plates using an edge-based MITC3 finite elements, *Composites Part B: Engineering*, 107, 2016, 162-173.
[16] Mantari, J., Monge, J., Free vibration and bending analysis of functionally graded sandwich plates based on an optimized hyperbolic unified formulation, *International Journal of Mechanical Sciences*, 119, 2016, 170-186.
[17] Xiang, S., Liu, Y.Q., An nth-order shear deformation theory for static analysis of functionally graded sandwich plates, *Journal of Sandwich Structures & Materials*, 18, 2016,579-596.
[18] Kashtalyan, M., Menshykova, M., Three-dimensional elasticity solution for sandwich panels with a functionally graded core, *Composite Structures*, 87, 2009, 36-43.
[19] Woodward, B., Kashtalyan, M., Bending response of sandwich panels with graded core: 3D elasticity analysis, *Mechanics of Advanced Materials and Structures*, 17, 2010, 586-594.
[20] Abdelaziz, H.H., Atmane, H.A., Mechab, I., Boumia, L., Tounsi, A., Adda Bedia, E.A., Static analysis of functionally graded sandwich plates using an efficient and simple refined theory, *Chinese Journal of Aeronautics*, 24, 2011, 434-448.
[21] Li, D., Deng, Z., Xiao, H., Zhu, L., Thermomechanical bending analysis of functionally graded sandwich plates with both functionally graded face sheets and functionally graded cores, *Mechanics of Advanced Materials and Structures*, 25, 2018, 179-191.
[22] Thanh, C-L., Ferreira, A.J.M., Abdel Wahab, M., A refined size-dependent couple stress theory for laminated composite micro-plates using isogeometric analysis, *Thin–Walled Structures*, 145, 2019, 106427
[23] Phung-Van, P., Tran, L.V., Ferreira, A.J.M., Nguyen-Xuan, H., Abdel-Wahab, M., Nonlinear transient isogeometric analysis of smart piezoelectric functionally graded material plates based on generalized shear deformation theory under thermo-electro-mechanical loads, *Nonlinear Dynamics*, 87, 879–894.
[24] Phung-Van, P., Thai, C-H., Nguyen-Xuan, H., Abdel-Wahab, M., An isogeometric approach of static and free vibration analyses for porous FG nanoplates, *European Journal of Mechanics / A Solids*, 78, 2019, 103851.
[25] Phung-Van, P., Thai, C-H., Nguyen-Xuan, H., Abdel-Wahab, M., Porosity-dependent nonlinear transient responses of functionally graded nanoplates using isogeometric analysis, *Composites Part B*, 164, 2019, 215-225.
[26] Thai, C-H., Ferreira, A.J.M., Rabczuk, T., Nguyen-Xuan, H., Size-dependent analysis of FG-CNTRC microplates based on modified strain gradient elasticity theory, *European Journal of Mechanics / A Solids*, 72, 2018, 521-538.
[27] Thanh C-L., Phung-Van, P., Thai, C-H., Nguyen-Xuan, H., Abdel-Wahab, M., Isogeometric analysis of functionally graded carbon nanotube reinforced composite nanoplates using modified couple stress theory, *Composite Structures*, 184, 2018, 633-649.
[28] Neves, A.M.A., Ferreira, A.J.M., Carrera, E., Cinefra, M., Roque, C.M.C., Jorge, R.M.N., Soares, C.M.M., Static, free vibration and buckling analysis of isotropic and sandwich functionally graded plates using a quasi-3D higher-order shear deformation theory and a meshless technique, *Composites Part B: Engineering*, 44, 2013, 657-674.
[29] Demirhan, P.A., Taskin, V., Levy solution for bending analysis of functionally graded sandwich plates based on four variable plate theory, *Composite Structures*, 177, 2017, 80-95.
[30] Moradi-Dastjerdi, R., Aghadavoudi, F., Static analysis of functionally graded nanocomposite sandwich plates reinforced by defected CNT, *Composite Structures*, 200, 2018, 839-848.
[31] Li, D., Deng, Z., Xiao, H., Jin, P., Bending analysis of sandwich plates with different face sheet materials and functionally graded soft core, *Thin-Walled Structures*, 122, 2018, 8-16.
[32] Thai, C-H., Ferreira, A.J.M., Nguyen-Xuan, H., Isogeometric analysis of size-dependent isotropic and sandwich functionally graded microplates based on modified strain gradient elasticity theory, *Composite Structures*, 192, 2018, 274-288.
[33] Phung-Van, P., Thanh, C-L., Nguyen-Xuan, H., Abdel-Wahab, M., Nonlinear transient isogeometric analysis of FG-CNTRC nanoplates in thermal

environments, *Composite Structures*, 201, 2018, 882-892.

[34] Thanh, C-L., Tran, L-V., Bui, T.Q., Nguyen, H.X., Abdel-Wahab, M., Isogeometric analysis for size-dependent nonlinear thermal stability of porous FG microplates, *Composite Structures*, 221, 2019, 110838.

[35] Daikh, A.A., Zenkour, A.M., Effect of porosity on the bending analysis of various functionally graded sandwich plates, *Materials Research Express*, 6, 2019, 065703.

[36] Cao, Z-Y., Tang, S-G., Cheng, G-H., 3D analysis of functionally graded material plates with complex shapes and various holes, *Applied Mathematics and Mechanics: English Edition*, 30(1), 2009, 13–18.

[37] Rezaei, R., Shaterzadeh, A.R., Abolghasemi, S., Buckling analysis of rectangular functionally graded plates with an elliptic hole under thermal loads, *Journal of Solid Mechanics*, 7(1), 2015, 41–57.

[38] Yang, B., Chen, W.Q., Ding, H.J., 3D elasticity solutions for equilibrium problems of transversely isotropic FGM plates with holes, *Acta Mechanica*, 226, 2015, 1571–1590.

[39] Yang, B., Chen, W.Q., Ding, H.J., Equilibrium of transversely isotropic FGM plates with an elliptical hole: 3D elasticity solutions, *Archive of Applied Mechanics*, I86, 2016, 1391–1414.

[40] Ansari, R., Faghih Shojaei, M., Shahabodini, A., Bazdid-Vahdati, M., Three-dimensional bending and vibration analysis of functionally graded nanoplates by a novel differential quadrature-based approach, *Composite Structures*, 131, 2015, 753-764.

[41] Ansari, R., Torabi, J., Norouzzadeh, A., Bending analysis of embedded nanoplates based on the integral formulation of Eringen's nonlocal theory using the finite element method, *Physica B: Condensed Matter*, 534, 2018, 90–97.

[42] Sobhy, M., A comprehensive study on FGM nanoplates embedded in an elastic medium, *Composite Structures*, 134, 2015, 966-980.

[43] Salehipour, H., Nahvi, H., Shahidi, A.R., Mirdamadi, H.R., 3D elasticity analytical solution for bending of FG micro/nanoplates resting on elastic foundation using modified couple stress theory, *Applied Mathematical Modelling*, 47, 2017, 174-188.

[44] Kolahchi, R., Moniri Bidgoli, A.M., Heydari, M.M., Size-dependent bending analysis of FGM nano-sinusoidal plates resting on orthotropic elastic medium, *Structural Engineering and Mechanics*, 55(5), 2015, 1001-1014.

[45] Arefi, M., Zenkour, A.M., Size-dependent electro-magneto-elastic bending analyses of the shear-deformable axisymmetric functionally graded circular nanoplates, *The European Physical Journal Plus*, 132(423), 2017, 1-13.

[46] Lim, C., Zhang, G., Reddy, J.N., A higher-order nonlocal elasticity and strain gradient theory and its applications in wave propagation, *Journal of the Mechanics and Physics of Solids*, 78, 2015, 298-313.

[47] Eringen, A.C., On differential equations of nonlocal elasticity and solutions of screw dislocation and surface waves, *Journal of Applied Physics*, 54, 1983, 4703-4710.

[48] Ebrahimi, F., Barati, M.R., Dabbagh, A., A nonlocal strain gradient theory for wave propagation analysis in temperature-dependent inhomogeneous nanoplates, *International Journal of Engineering Science*, 107, 2016, 169-182.

[49] Reddy, J.N., A general non-linear third order theory of plates with moderate thickness, *International Journal of Non-linear Mechanics*, 25, 1990, 677-686.

[50] Touratier, M., An efficient standard plate theory, *International Journal of Engineering Science*, 29, 1991, 901-916.

[51] Senthilnathan, N.R., Lim, S.P., Lee, K.H., Chow, S.T., Buckling of shear-deformable plates, *AIAA Journal*, 25, 1987, 1268-1271.

[52] Thai, H.T., Nguyen, T.K., Vo, T.P., Lee, J., Analysis of functionally graded sandwich platesusing a new first-order shear deformation theory, *European Journal of Mechanics-A/Solids*, 45, 2014, 211-225.

[53] Zenkour, A. M., A comprehensive analysis of functionally graded sandwich plates: Part 2—Buckling and free vibration, *International Journal of Solids and Structures*, 42, 2005, 5243-5258.

[54] Daikh, A.A., Temperature dependent vibration analysis of functionally graded sandwich plates resting on Winkler/Pasternak/Kerr foundation, *Materials Research Express*, 6, 2019, 065702.

[55] Nguyen-Xuan, H., Thai, C.H., Nguyen-Thoi, T., Isogeometric finite element analysis of composite sandwich plates using a higher order shear deformation theory, *Composites Part B: Engineering*, 55, 2013, 558-74.

[56] Nguyen, T.N., Thai, C.H., Nguyen-Xuan, H., On the general framework of high-order shear deformation theories for laminated composite plate structures: A novel unified approach, *International Journal of Mechanical Sciences*, 110, 2016, 242-255.

ORCID iD

Ahmed Amine Daikh https://orcid.org/0000-0002-4666-2750
Ashraf M. Zenkour https://orcid.org/0000-0002-0883-8073